Mechanistic understanding of sodium storage from operando stress measurements in hard-carbon thin-films

Akshay S. Pakhare[1,*], Naba. K. Karan[2,3], Pradeep. R. Guduru[1]

[1]School of Engineering, Brown University, Providence, RI, 02906 USA
[2]Department of Materials Science and Engineering, [3]Center for Clean Energy Engineering, University of Connecticut, Storrs, CT 06269 USA

Abstract

Hard carbon is a promising anode material for sodium-ion batteries, yet the sodium-storage mechanism in hard carbon remains debated. Here, operando substrate-curvature measurements on hard-carbon thin films were used to probe the volume-expansion-induced stress during sodiation and desodiation. The volume-expansion-induced stress rises steeply in the higher-voltage sloping region during initial sodiation, then it increases at a slower rate in the low-voltage plateau region, followed by a second steep slope below approximately 0.025 V at the end of sodiation. These regimes in stress evolution are consistent with intercalation-dominated storage in the sloping region, pore filling or adsorption in the plateau region, and a plating process at low potentials. The stress relaxation profile evolves asymmetrically during desodiation, indicating that sodium removal from hard carbon is not a simple reversal of sodium insertion into it. The irreversibility in sodiation-desodiation profiles of hard carbon is associated with sodium retention and/or (micro)structural rearrangement.

Keywords: Sodium-ion batteries; hard carbon; operando stress measurement; sodium-storage mechanism; thin film electrodes

1 Introduction

Hard carbon is a promising anode material for sodium-ion batteries as it combines a low working potential, useful reversible capacity, and better cyclability than many other candidate materials [1–5]. However, a complete understanding of the sodium storage mechanism in hard carbon anodes is lacking at present. The galvanostatic sodiation/desodiation response in hard carbons is typically divided into a higher-voltage sloping region and a low-voltage plateau region. However, a consensus has not yet been reached on the physical mechanistic origin of these distinct regions [4–10].

* Corresponding author. Email address: akshay_pakhare@brown.edu

The mechanistic assignments in the hard-carbon literature have been inferred from experimental signatures using a variety of in-situ/ex-situ analytical techniques at different states of charge. Physical processes including sodium insertion/intercalation, adsorption, pore-filling, pseudo-plating and combinations thereof have been proposed to be responsible for multistage sodium uptake in defect-rich and nanoconfined hard carbon environments. More importantly though, quite disparate and conflicting processes have been assigned for sodiation in the same voltage region. Stevens and Dahn [4] used in-situ wide-angle X-ray scattering and showed that sodiation increased the interlayer spacing of disordered carbons in the sloping-voltage region, which they interpreted as sodium insertion between graphene-like layers, while the low-voltage capacity was associated with filling of pore volume. Whereas, the adsorption was assigned to be the primary mechanism in the sloping-voltage region by Qiu et al. [6] based on in-situ XRD, ex-situ NMR, and EPR measurements. Gotoh et al. [7] used solid-state ^{23}Na NMR and resolved distinct sodium environments in hard carbon, which they assigned to sodium stored between disordered graphene sheets and sodium located in closed nanopores, supporting the presence of multiple sodium storage sites. Bai et al. [8] provided more direct evidence for the plateau assignment by filling micropores with sulfur and showing that the low-voltage plateau was suppressed, which linked that portion of the capacity to pore filling. By contrast, operando Raman measurements by Weaving et al. [9] showed a substantial reversible evolution in G-band position that tracked the sloping region, which they interpreted as intercalation within turbostratic carbon layers. More recently, Eren et al. [10] combined operando small-angle X-ray scattering and Raman spectroscopy characterization with electrochemical analysis and proposed a refined three-stage picture in which the sloping region is dominated by fast capacitive uptake, the early plateau by faradaic storage at micropore inner surfaces, and the late plateau by quasi-metallic sodium accumulation in pores. Taken together, these studies on composite electrodes highlight that the debate over a complete mechanistic understanding of (de)sodiation in hard carbon anodes persists not because the field lacks evidence, but because different techniques interrogate different signatures of sodium storage, and an independent measurement that directly reflects the associated volume-change response has remained largely unexplored in dense hard-carbon films. Thus, the key issue that remains unresolved is to determine which physical processes govern the sloping and plateau regions and how these contributions can be distinguished using an independent physical observable.

A direct consequence of sodium storage in hard carbon is its volume change. Sodium uptake into hard carbon alters the local atomic packing through occupation of defects, interlayer space, and pore space, and several recent studies have shown that this process is accompanied by measurable volume changes [11–14]. When this expansion is mechanically constrained, it generates stress. Operando stress measurements, therefore, offer a route to probing sodium storage mechanisms through its mechanical signature, as has been shown previously for other battery electrodes, such as composite Li-Ion battery electrodes [15–18] and, more recently, for hard carbon composite anodes for Na-ion batteries [19–21]. However, stress measurements in composite electrodes necessarily reflect not only the response of the hard carbon itself, but also the influence of interparticle pores, binder, conductive additives, and the mechanical constraint on them. In this work, we overcome that limitation by using hard carbon thin films as a geometrically simple model

system and quantify the in-plane stress generated in them during sodiation and desodiation by operando substrate curvature measurements. This configuration enables the observed stress changes to be related more directly to volume expansion in hard carbon itself, thereby providing an independent basis for identifying the dominant sodium storage mechanisms.

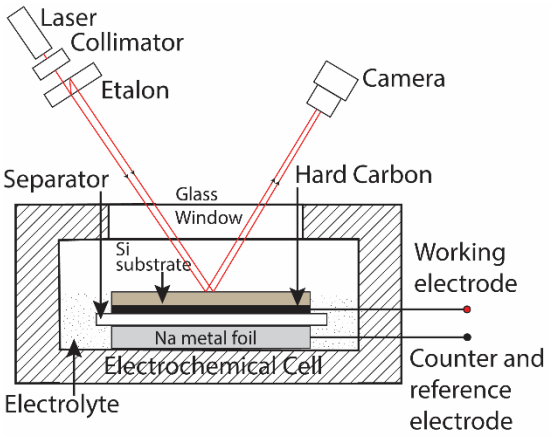

Fig. 1 Schematic of the operando substrate-curvature measurement setup used to monitor stress evolution in the hard-carbon thin films during electrochemical cycling. The hard-carbon-coated Si substrate serves as the working electrode, while sodium metal serves as the counter/reference electrode. During sodiation and desodiation, sodium-storage-induced volume expansion or contraction changes the substrate curvature, which is tracked by the multibeam optical sensor through the change in reflected laser-spot spacing

2 Experimental Method

2.1 Hard carbon thin film preparation

Hard-carbon thin films were prepared by pyrolysis of a sucrose-derived precursor on Si wafers. A 100 nm Cr layer was first deposited by DC magnetron sputtering on the unpolished side of 25.4 mm x 25.4 mm, 500 μm thick Si (100) wafers to serve as the current collector. A precursor solution containing 36.75 wt.% sucrose, 36.75 wt.% acetic acid, 9.62 wt.% polyethylene glycol, and 16.89 wt.% methoxyethanol was then spin-coated (~2000 rpm) onto the substrate and dried in air. The coated wafers were pyrolyzed under Ar by heating to 1000 °C at 5 °C min^{-1}, holding at 1000 °C for 1 h, and then allowing the furnace to cool naturally to room temperature. The resulting hard carbon films, as evidenced by Raman measurements, were uniform and dense, with a thickness of approximately 2 μm.

2.2 Electrochemical Measurements

Electrochemical cycling was carried out in a custom cell (schematically shown in Fig. 1) designed to carry out simultaneous stress measurement by the substrate curvature method. Sodium metal serves as both the counter and reference electrodes, and the hard-carbon-coated Si substrate

serves as the working electrode. A Whatman glass fiber separator was placed between the electrodes, and the liquid electrolyte used was 1 M $NaClO_4$ in propylene carbonate containing 5 wt% fluoroethylene carbonate. To avoid interference with the optical measurement, the liquid electrolyte level was maintained below the top surface of the substrate. Galvanostatic cycling was performed between 2.0 and 0.001 V (versus Na/Na^+) at a current density of 0.16 μA cm^{-2} (approximately C/20). Cyclic voltammetry was carried out at a scan rate of 0.25 mV s^{-1} between 2 V and 1 mV.

2.3 Operando stress measurement

Stress evolution during sodiation and desodiation was measured by operando substrate-curvature monitoring using a multibeam optical sensor (MOS, k-Space Associates), following the general approach used previously for battery electrodes (Sethuraman et al., 2012). A 2 × 2 laser-beam array is reflected from the back surface of the substrate onto a CCD camera, and the relative change in spot spacing during cycling was used to determine the substrate curvature. The curvature change κ was calculated from the relative change in laser spot spacing according to

$$\kappa = \frac{1}{A_m} \frac{d - d_0}{d_0} \quad (1)$$

where d_0 is the initial laser spot spacing, d is the instantaneous spot spacing and A_m is the calibrated mirror constant of the optical setup. The biaxial film stress σ, is then obtained using the Stoney equation [22],

$$\sigma = \frac{M_s h_s^2}{6 h_f} \kappa \quad (2)$$

where $M_s = E_s/(1 - \nu_s)$ is the biaxial modulus of Si substrate, h_s is the substrate thickness, and h_f is the film thickness.

3 Results and Discussion

Representative planar (Figure 2a) and cross-sectional (2b) scanning electron micrographs of show that the pyrolyzed hard-carbon thin film is continuous and uniform over the Si substrate and has a thickness of 2.18 µm ± 0.41 µm. This geometry provides a mechanically simple platform for operando stress measurements because the measured curvature response can be related directly to the in-plane stress generated by sodiation-induced volume change in the hard carbon film, without the additional structural averaging associated with composite porosity, binder deformation, or particle-particle interactions.

Raman spectroscopy was performed on the synthesized hard-carbon thin film to assess the carbon structure after pyrolysis. The film exhibits an I_D/I_G Raman intensity ratio of 1.0, as shown in Fig.3a, consistent with sucrose-derived hard carbon pyrolyzed at 1000 °C [2]. This ratio indicates a disordered, non-graphitic carbon framework containing short-range graphitic domains. This interpretation is also consistent with the broader structural picture of hard carbon, which comprises graphitic domains separated by disordered regions and nanoporous space, with the relative fraction of each governed strongly by heat-treatment temperature [23].

The electrochemical response of the hard-carbon thin film is shown in Fig. 3b, c and d. In cyclic voltammetry (Fig.3b), the first cathodic sweep exhibits a broad irreversible reduction feature centered near 1.25 V, which is attributed to solid interphase formation (SEI) on the initially fresh carbon surface. The SEI feature appears over a similar potential range as that reported for comparable composite hard carbon electrodes with the same electrolyte chemistry, where Chanda et al. [19] observed it between 1.4 and 0.8 V. Some variation is expected, because SEI formation depends on carbon surface structure and morphology, as shown by Peled et al. [24] and Luchkin et al.[25]. In the present case, the difference likely reflects the contrast between the planar thin-film surface and particulate composite electrodes' morphologies. Further reduction near 0.1 V corresponds to sodiation of hard carbon, whereas the anodic feature near 0.4 V corresponds to desodiation [4,26–28]. The galvanostatic response as a function of time and capacity (Fig. 3 c, d) shows the characteristic two-region behavior that is typically reported for hard carbon anodes. It consists of a sloping region above about 0.1 V followed by a low voltage plateau below about 0.1 V [1,2,4]. The dotted vertical line in Fig. 3c and 3d separates these two regions. The capacity associated with the plateau region is smaller than that associated with the sloping region, indicating that sodium storage in the 1000 °C hard-carbon thin film is dominated by the higher-potential sloping-region.

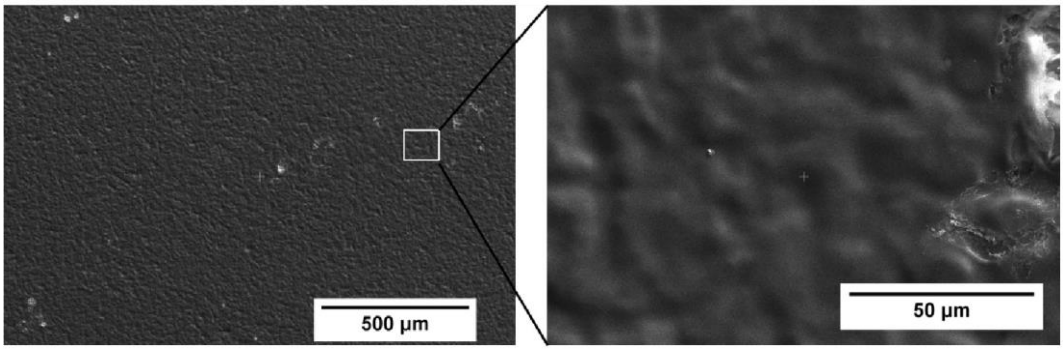

(a)

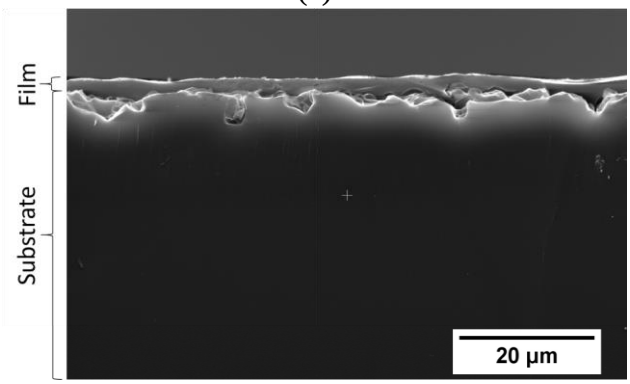

(b)

Fig. 2 (a) Top-down SEM image showing a continuous hard-carbon film formed on the unpolished side of the Si wafer after pyrolysis. The inset shows a higher-magnification view of the surface morphology, where the apparent waviness follows results from the roughness of the underlying Si

substrate. (b) Cross-sectional SEM image showing a dense hard-carbon film on the Si substrate, with a measured thickness of approximately 2.18 ± 0.41 µm

The first-cycle coulombic efficiency is approximately 60%, increasing to about 80% in the subsequent cycles as determined from the capacity profiles in Fig. 3d. This behavior is consistent with irreversible sodium consumption during initial SEI formation, together with incomplete reversibility of the plateau-region storage process. One possible contribution to this irreversibility is trapping of sodium within the hard-carbon structure. Incomplete reversal may also arise from sodium retention in closed pores. Because the plateau region has been associated with metallic-cluster-like sodium filling of closed pores, sodium removal from these nanoconfined sites may be kinetically hindered during desodiation [29]. The comparatively weaker plateau during desodiation therefore indicates that low-voltage sodium removal does not occur as a simple mirror-image reversal of sodiation, but instead reflects the asymmetric emptying of pore-associated storage sites [10,20,29].

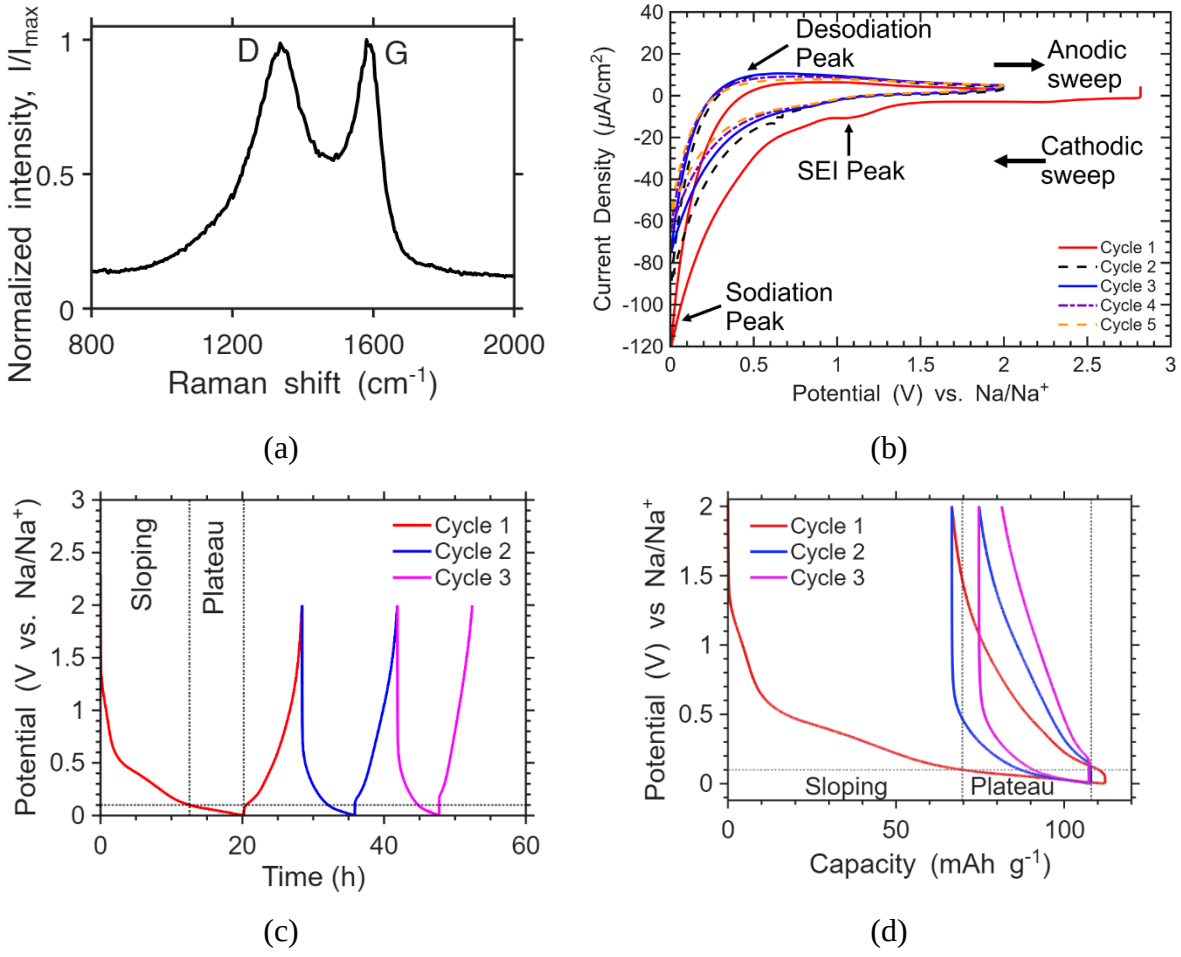

Fig. 3 (a) Raman spectrum of the sucrose-derived hard-carbon thin film pyrolyzed at 1000 °C, showing the characteristic D and G bands used to assess disorder and short-range graphitic ordering. (b) Cyclic voltammetry response measured at 0.25 mV s^{-1}. The first cathodic sweep

shows an irreversible reduction feature associated with SEI formation, followed by lower potential sodiation and the corresponding anodic desodiation response. (c) Galvanostatic sodiation and desodiation profiles plotted as a function of time for the first three cycles at 0.16 μA cm^{-2}, corresponding to approximately C/20. (d) The same galvanostatic data plotted as a function of capacity. The response shows the characteristic hard-carbon sloping region at higher potential and low-voltage plateau region near the end of sodiation, with the plateau contribution becoming less pronounced after the first cycle. The dashed lines are drawn to aid visualization of regimes with different slopes in the voltage profile during first sodiation

Figure 4a and 4b shows the biaxial stress evolution of the hard-carbon film together with the corresponding electrode potential during sodiation and desodiation. Stress arises from sodiation-induced volume expansion of the hard-carbon film under in-plane constraint from the Si substrate. During the first sodiation cycle, the film develops compressive stress as sodium is stored in the carbon structure. The stress evolution does not follow a single constant slope. Instead, three features are resolved as the potential decreases: a steep compressive stress rise in the higher-voltage sloping region, a slower compressive stress increase in the low-voltage plateau region, and an additional change in stress evolution below approximately 0.025 V near the end of sodiation. These regimes are segmented in Fig. 4a and highlighted in different colors in Fig. 4c for the first sodiation half-cycle. The maximum compressive stress reaches approximately 0.12 GPa, showing that sodium uptake in the dense hard carbon film produces a substantial volume-expansion response. During desodiation, the stress relaxes toward lower compression, but the unloading path does not retrace the sodiation path. Two unloading regimes are observed: a smaller-magnitude stress change below approximately 0.15 V and a larger-magnitude stress change between approximately 0.15 V and 2.0 V shown in Fig. 4a and 4b. The asymmetry in stress evolution indicates that sodium removal does not occur as a simple mirror-image reversal of sodium insertion in hard carbon anodes. The feature below 0.025 V that appears during sodiation is not clearly resolved during desodiation, suggesting that the underlying process in this region is predominantly irreversible. As shown in Fig. 4b, the stress also does not return fully to its initial value at the end of desodiation (2.0 V cutoff), leaving a residual compressive stress of approximately 13 MPa that may be attributed to sodium retained in the hard-carbon structure, irreversible structural rearrangement during the first sodiation, or both.

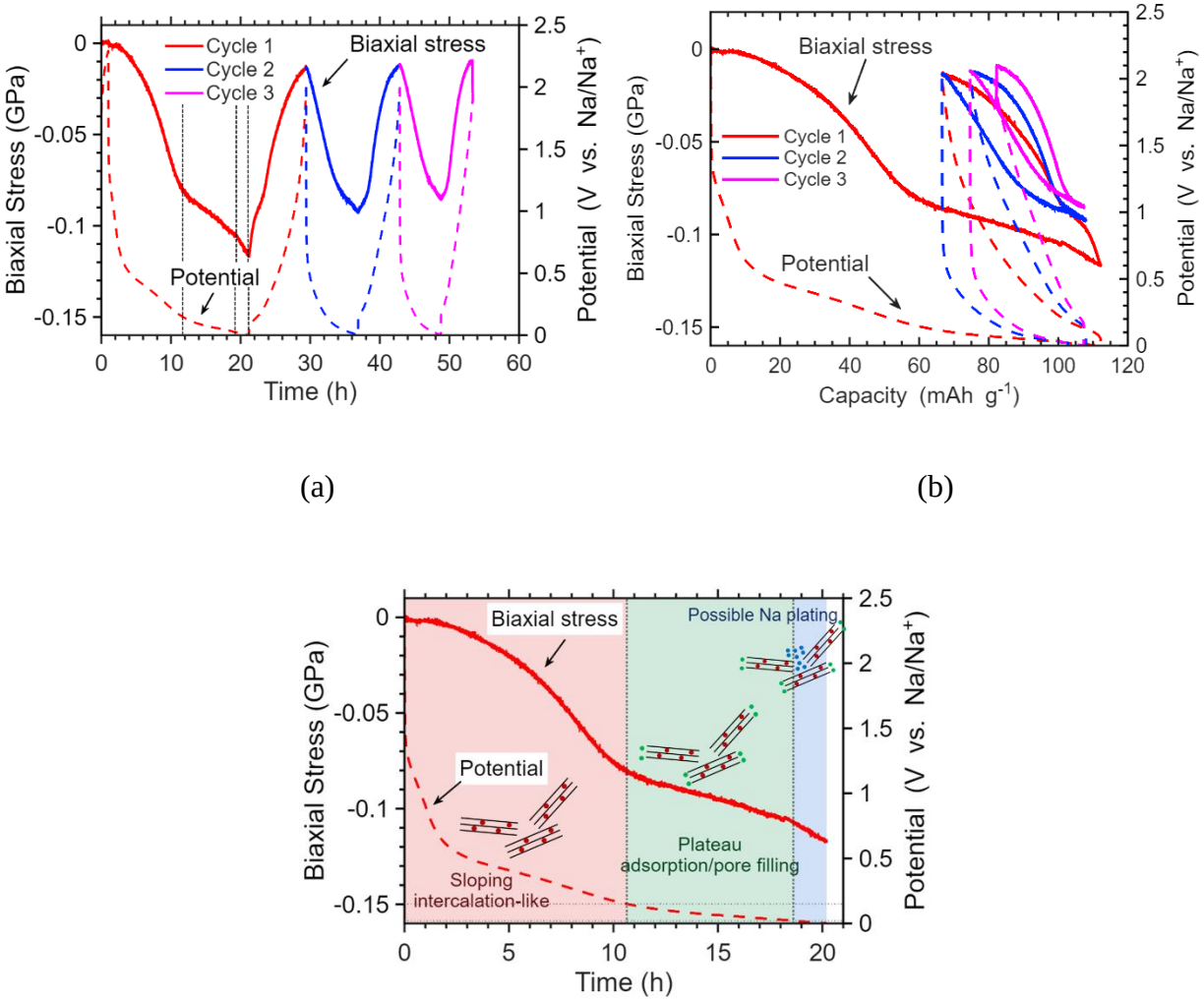

Fig. 4 (a) Biaxial stress and electrode potential plotted as a function of time for the first three cycles. The solid curves represent biaxial stress, and the dashed curves represent electrode potential. During sodiation, sodium storage produces compressive stress in the film, with changes in the stress response corresponding to different regions of the potential profile. (b) The biaxial stress and potential response as function of capacity. (c) Enlarged first-cycle sodiation response, segmented into mechanically distinct storage regimes. The red, green, and blue shaded regions correspond to intercalation-dominated storage in the sloping region, pore filling or adsorption in the plateau region, and a plating-consistent process at very low potential, respectively. The schematics use the same color scheme to identify sodium associated with each mechanism: red for intercalation, green for pore filling or adsorption, and blue for plating-consistent sodium accumulation

The subsequent cycles in Fig. 4a and 4b retain the main stress-potential coupling but with a weaker low-voltage contribution. During cycles 2 and 3, sodiation again shows a larger stress

change in the higher-voltage sloping region followed by a smaller stress change in the low-voltage plateau region. During desodiation, the lower-slope response near 0.1–0.15 V and the higher-slope response above approximately 0.15 V are again observed. However, the very-low-voltage feature below approximately 0.025 V is much less pronounced or absent after the first cycle. This behavior parallels the electrochemical response in Fig. 3d, where the plateau contribution also diminishes after the first cycle. The repeated high-slope stress response indicates that intercalation-dominated storage remains active during cycling, whereas the weakening of the lower-voltage stress features suggests that pore filling, adsorption, or plating-consistent storage contributes less to the macroscopic volume change after the first sodiation. This reduced contribution may reflect partial saturation of pore or defect sites, sodium trapping, or structural evolution of the hard-carbon film during the first cycle.

Figure 4c segments the first-cycle sodiation response into mechanically distinct storage regimes identified from Fig. 4a and 4b, thus schematically illustrating the corresponding sodium-storage processes. In the higher-voltage sloping region, the stress rises most steeply, indicating that the largest incremental volume expansion during sodium uptake. This regime is assigned to intercalation-dominated sodium storage in graphitic or pseudo-graphitic domains, as shown schematically by sodium atoms (red dots) inserted between graphitic layers in Fig. 4c. This assignment is consistent with the fact that sodium insertion into the carbon framework produces a larger dimensional response than storage in pore volume. A similar correspondence between intercalation and stress evolution was reported previously for graphite during lithiation, where staging-related insertion produces pronounced biaxial stress changes [15,16]. We also note that the possibility of adsorption in this steep slope region cannot be fully ruled out from the observed stress evolution profile. The stress response in this region might arise from simultaneous intercalation and adsorption. It suggests that intercalation dominates in this region and further sodiation beyond this region does not involve intercalation. As sodiation proceeds into the low-voltage plateau region, the compressive stress continues to increase but with a markedly smaller slope. This lower rate of stress evolution indicates a storage process with smaller incremental volume expansion with further sodium storage, which is assigned to pore filling or adsorption in nanoconfined carbon environments. This process is represented schematically in Fig. 4c by sodium stored at pore surfaces or within confined pore regions, rather than inserted between graphitic layers. This interpretation is supported by prior operando dilatometry and substrate-curvature measurements on composite hard-carbon electrodes, where the plateau region was associated with a reduced dimensional or stress response per unit stored charge [4,10,19,30]. Below approximately 0.025 V, the stress changes slope again before the 0.001 V sodiation cutoff. This third feature is mechanically distinct from the preceding plateau response and is consistent with an additional very-low-voltage process involving sodium plating. In the schematic, this regime is represented by more localized sodium accumulation within confined pore regions, consistent with a plating-like or metal-like sodium storage process discussed in prior dilatometry studies of hard carbon [12]. The key new observation in the present work from the dense thin-film experiments is that three distinct regimes are resolved directly from the stress response: intercalation in the sloping region,

pore filling or adsorption in the plateau region, and a plating-consistent process near the end of sodiation.

4 Conclusion

In summary, operando substrate-curvature measurements on hard-carbon thin films reveal that sodium storage proceeds through mechanically distinct regimes with different volume-expansion signatures. The steep rise in compressive stress in the higher-voltage sloping region indicates the largest volume change and is attributed to sodium intercalation into graphitic domains, although simultaneous contribution from pore filling cannot be ruled out. As sodiation proceeds into the low-voltage plateau region, the stress continues to increase but with a smaller slope, indicating a storage process with smaller incremental volume change, which is consistent with pore filling and adsorption in nanoconfined carbon environments. A further increase in stress slope at the end of first sodiation indicates the onset of an additional low-voltage process, which is assigned here to sodium plating. During desodiation, the asymmetric stress change shows that these processes are not reversed in a simple mirror-image manner possibly due to sodium trapping in defect sites. Taken together, sodium storage in the hard-carbon thin film proceeds through intercalation dominated in the sloping region, pore filling or adsorption in the plateau region, and a plating-consistent process at the end of sodiation, followed by asymmetric and partially irreversible sodium removal during desodiation.

Statements and Declarations

CRediT authorship contribution statement

Akshay S. Pakhare.: Methodology, Investigation, Formal analysis, Writing—Original draft. Naba K. Karan: Conceptualization, Formal analysis, Validation, Writing—Review and Editing. Pradeep R. Guduru: Conceptualization, Supervision, Resources, Methodology, Writing—Review and Editing. All authors read and approved the final manuscript

Acknowledgments

Financial support from the Office of Naval Research is gratefully acknowledged (grant #N00014-21-1-2815 and #N00014-23-1-2688).

Competing interests

The authors declare that they have no relevant financial or non-financial interests to disclose.

Data availability

The data supporting the findings of this study are available from the corresponding author upon reasonable request.

Declaration of generative AI and AI-assisted technologies in the manuscript preparation process

During the preparation of this work, the authors used ChatGPT for grammar correction and sentence structure improvement. Subsequently, the authors reviewed and edited the content as needed and take full responsibility for the content of the published article.

References

[1] S. Komaba, W. Murata, T. Ishikawa, N. Yabuuchi, T. Ozeki, T. Nakayama, A. Ogata, K. Gotoh, K. Fujiwara, Electrochemical Na Insertion and Solid Electrolyte Interphase for Hard-Carbon Electrodes and Application to Na-ion Batteries, Advanced Functional Materials 21 (2011) 3859–3867. https://doi.org/10.1002/adfm.201100854.

[2] K. Kubota, S. Shimadzu, N. Yabuuchi, S. Tominaka, S. Shiraishi, M. Abreu-Sepulveda, A. Manivannan, K. Gotoh, M. Fukunishi, M. Dahbi, S. Komaba, Structural Analysis of Sucrose-Derived Hard Carbon and Correlation with the Electrochemical Properties for Lithium, Sodium, and Potassium Insertion, Chem. Mater. 32 (2020) 2961–2977. https://doi.org/10.1021/acs.chemmater.9b05235.

[3] A. Rudola, A.J.R. Rennie, R. Heap, S.S. Meysami, A. Lowbridge, F. Mazzali, R. Sayers, C.J. Wright, J. Barker, Commercialisation of high energy density sodium-ion batteries: Faradion's journey and outlook, J. Mater. Chem. A 9 (2021) 8279–8302. https://doi.org/10.1039/D1TA00376C.

[4] D.A. Stevens, J.R. Dahn, The Mechanisms of Lithium and Sodium Insertion in Carbon Materials, J. Electrochem. Soc. 148 (2001) A803. https://doi.org/10.1149/1.1379565.

[5] P. Voß, B. Gruber, M. Mitterfellner, J.-D. Plöpst, F. Degen, R. Schmuch, S. Lux, Benchmarking state-of-the-art sodium-ion battery cells – modeling energy density and carbon footprint at the gigafactory-scale, Energy & Environmental Science 18 (2025) 8104–8129. https://doi.org/10.1039/D5EE00415B.

[6] S. Qiu, L. Xiao, M.L. Sushko, K.S. Han, Y. Shao, M. Yan, X. Liang, L. Mai, J. Feng, Y. Cao, X. Ai, H. Yang, J. Liu, Manipulating Adsorption–Insertion Mechanisms in Nanostructured Carbon Materials for High-Efficiency Sodium Ion Storage, Advanced Energy Materials 7 (2017) 1700403. https://doi.org/10.1002/aenm.201700403.

[7] K. Gotoh, T. Ishikawa, S. Shimadzu, N. Yabuuchi, S. Komaba, K. Takeda, A. Goto, K. Deguchi, S. Ohki, K. Hashi, T. Shimizu, H. Ishida, NMR study for electrochemically inserted Na in hard carbon electrode of sodium ion battery, Journal of Power Sources 225 (2013) 137–140. https://doi.org/10.1016/j.jpowsour.2012.10.025.

[8] P. Bai, Y. He, X. Zou, X. Zhao, P. Xiong, Y. Xu, Elucidation of the Sodium-Storage Mechanism in Hard Carbons, Advanced Energy Materials 8 (2018) 1703217. https://doi.org/10.1002/aenm.201703217.

[9] J.S. Weaving, A. Lim, J. Millichamp, T.P. Neville, D. Ledwoch, E. Kendrick, P.F. McMillan, P.R. Shearing, C.A. Howard, D.J.L. Brett, Elucidating the Sodiation Mechanism in Hard Carbon by Operando Raman Spectroscopy, ACS Appl. Energy Mater. 3 (2020) 7474–7484. https://doi.org/10.1021/acsaem.0c00867.

[10] E.O. Eren, E. Senokos, E. Scoppola, Z. Song, M. Antonietti, P. Giusto, An enhanced three-stage model for sodium storage in hard carbons, Energy Environ Sci 18 (2025) 7859–7868. https://doi.org/10.1039/d4ee06029f.

[11] D. Chen, W. Zhang, K. Luo, Y. Song, Y. Zhong, Y. Liu, G. Wang, B. Zhong, Z. Wu, X. Guo, Hard carbon for sodium storage: mechanism and optimization strategies toward commercialization, Energy Environ. Sci. 14 (2021) 2244–2262. https://doi.org/10.1039/D0EE03916K.
[12] I. Escher, G. A. Ferrero, M. Goktas, P. Adelhelm, In Situ (Operando) Electrochemical Dilatometry as a Method to Distinguish Charge Storage Mechanisms and Metal Plating Processes for Sodium and Lithium Ions in Hard Carbon Battery Electrodes, Adv Materials Inter 9 (2022) 2100596. https://doi.org/10.1002/admi.202100596.
[13] J. Li, C. Peng, J. Li, J. Wang, H. Zhang, Insight into Sodium Storage Behaviors in Hard Carbon by ReaxFF Molecular Dynamics Simulation, Energy Fuels 36 (2022) 5937–5952. https://doi.org/10.1021/acs.energyfuels.2c00575.
[14] K. Wang, Y. Xu, Y. Li, V. Dravid, J. Wu, Y. Huang, Sodium storage in hard carbon with curved graphene platelets as the basic structural units, J. Mater. Chem. A 7 (2019) 3327–3335. https://doi.org/10.1039/C8TA11510A.
[15] A. Mukhopadhyay, A. Tokranov, X. Xiao, B.W. Sheldon, Stress development due to surface processes in graphite electrodes for Li-ion batteries: A first report, Electrochimica Acta 66 (2012) 28–37. https://doi.org/10.1016/j.electacta.2012.01.058.
[16] V.A. Sethuraman, N. Van Winkle, D.P. Abraham, A.F. Bower, P.R. Guduru, Real-Time Stress Measurements in Lithium-Ion Battery Negative-Electrodes, Journal of Power Sources 206 (2012) 334–342. https://doi.org/10.1016/j.jpowsour.2012.01.036.
[17] V.A. Sethuraman, A. Nguyen, M.J. Chon, S.P.V. Nadimpalli, H. Wang, D.P. Abraham, A.F. Bower, V.B. Shenoy, P.R. Guduru, Stress Evolution in Composite Silicon Electrodes during Lithiation/Delithiation, Journal of The Electrochemical Society 160 (2013) A739–A746. https://doi.org/10.1149/2.021306jes.
[18] V.A. Sethuraman, V. Srinivasan, J. Newman, Analysis of Electrochemical Lithiation and Delithiation Kinetics in Silicon, Journal of The Electrochemical Society 160 (2013) A394–A403. https://doi.org/10.1149/2.008303jes.
[19] A. Chanda, A. Pakhare, A. Alfadhli, V.A. Sethuraman, S.P.V. Nadimpalli, Real-time measurement of sodiation induced stress in hard carbon composite electrodes, Journal of Power Sources 609 (2024) 234678. https://doi.org/10.1016/j.jpowsour.2024.234678.
[20] S. Mück, D. Kramer, K. Palanisamy, C. Kranz, R. Mönig, Mechanical Stress Reveals Asymmetry of Sodiation and Desodiation of Hard Carbon, ChemSusChem 18 (2025) e202501272. https://doi.org/10.1002/cssc.202501272.
[21] M. Yang, Z. Luo, X. Wang, X. Cao, W. Mao, Y. Pan, C. Dai, J. Pan, Revealing sodium storage mechanism of hard carbon anodes through in-situ investigation of mechano-electrochemical coupling behavior, Journal of Energy Chemistry 86 (2023) 227–236. https://doi.org/10.1016/j.jechem.2023.07.025.
[22] G.G. Stoney, The Tension of Metallic Films Deposited by Electrolysis, Proceedings of the Royal Society of London. Series A, Containing Papers of a Mathematical and Physical Character 82 (1909) 172–175. https://doi.org/10.1098/rspa.1909.0021.
[23] Z. T. Gossage, D. Igarashi, Y. Fujii, M. Kawaguchi, R. Tatara, K. Nakamoto, S. Komaba, New frontiers in alkali metal insertion into carbon electrodes for energy storage, Chemical Science 15 (2024) 18272–18294. https://doi.org/10.1039/D4SC03203A.
[24] E. Peled, D. Bar Tow, A. Merson, A. Gladkich, L. Burstein, D. Golodnitsky, Composition, depth profiles and lateral distribution of materials in the SEI built on HOPG-TOF SIMS and XPS studies, Journal of Power Sources 97–98 (2001) 52–57. https://doi.org/10.1016/S0378-7753(01)00505-5.

[25] S.Y. Luchkin, S.A. Lipovskikh, N.S. Katorova, A.A. Savina, A.M. Abakumov, K.J. Stevenson, Solid-electrolyte interphase nucleation and growth on carbonaceous negative electrodes for Li-ion batteries visualized with in situ atomic force microscopy, Sci Rep 10 (2020) 8550. https://doi.org/10.1038/s41598-020-65552-6.
[26] F. Wu, L. Liu, Y. Yuan, Y. Li, Y. Bai, T. Li, J. Lu, C. Wu, Expanding Interlayer Spacing of Hard Carbon by Natural K^+ Doping to Boost Na-Ion Storage, ACS Appl. Mater. Interfaces 10 (2018) 27030–27038. https://doi.org/10.1021/acsami.8b08380.
[27] Z. Zhu, W. Zhong, Y. Zhang, P. Dong, S. Sun, Y. Zhang, X. Li, Elucidating electrochemical intercalation mechanisms of biomass-derived hard carbon in sodium-/potassium-ion batteries, Carbon Energy 3 (2021) 541–553. https://doi.org/10.1002/cey2.111.
[28] Z. Zhu, F. Liang, Z. Zhou, X. Zeng, D. Wang, P. Dong, J. Zhao, S. Sun, Y. Zhang, X. Li, Expanded biomass-derived hard carbon with ultra-stable performance in sodium-ion batteries, J. Mater. Chem. A 6 (2018) 1513–1522. https://doi.org/10.1039/C7TA07951F.
[29] Z. Tang, R. Zhang, H. Wang, S. Zhou, Z. Pan, Y. Huang, D. Sun, Y. Tang, X. Ji, K. Amine, M. Shao, Revealing the closed pore formation of waste wood-derived hard carbon for advanced sodium-ion battery, Nat Commun 14 (2023) 6024. https://doi.org/10.1038/s41467-023-39637-5.
[30] Y. Jin, S. Sun, M. Ou, Y. Liu, C. Fan, X. Sun, J. Peng, Y. Li, Y. Qiu, P. Wei, Z. Deng, Y. Xu, J. Han, Y. Huang, High-Performance Hard Carbon Anode: Tunable Local Structures and Sodium Storage Mechanism, ACS Appl. Energy Mater. 1 (2018) 2295–2305. https://doi.org/10.1021/acsaem.8b00354.